Applied Physics Letters

RESEARCH ARTICLE | OCTOBER 20 2022

Aqueous-solution-synthesized gallium oxide dielectrics for high-mobility thin-film transistors enhanced by phosphorus incorporation

Special Collection: Metal Oxide Thin-Film Electronics

Wangying Xu ✉; Tao Peng; Lin Chen; ... et. al

Appl. Phys. Lett. 121, 163301 (2022)
https://doi.org/10.1063/5.0118814

Applied Physics Letters ARTICLE scitation.org/journal/apl

Aqueous-solution-synthesized gallium oxide dielectrics for high-mobility thin-film transistors enhanced by phosphorus incorporation

Cite as: Appl. Phys. Lett. **121**, 163301 (2022); doi: 10.1063/5.0118814
Submitted: 6 August 2022 · Accepted: 30 September 2022 ·
Published Online: 20 October 2022

Wangying Xu,[1,a)] Tao Peng,[2] Lin Chen,[2] Weicheng Huang,[1] Shuangmu Zhuo,[1] Qiubao Lin,[1] Chun Zhao,[3,a)] Fang Xu,[4] Yu Zhang,[5] and Deliang Zhu[2]

AFFILIATIONS

[1]Department of Physics, School of Science, Jimei University, Xiamen 361021, China
[2]College of Materials Science and Engineering, Shenzhen University, Shenzhen 518000, China
[3]Department of Electrical and Electronic Engineering, Xi'an Jiaotong-Liverpool University, Suzhou 215123, China
[4]Shenzhen Key Laboratory of Ultraintense Laser and Advanced Material Technology, Center for Advanced Material Diagnostic Technology, and College of Engineering Physics, Shenzhen Technology University, Shenzhen 518118, China
[5]Department of electronic and Communication Engineering, Shenzhen Polytechnic, Shenzhen 518055, China

Note: This paper is part of the APL Special Collection on Metal Oxide Thin-Film Electronics.
[a)]**Authors to whom correspondence should be addressed:** wyxu@jmu.edu.cn and chun.zhao@xjtlu.edu.cn

ABSTRACT

Gallium oxide (Ga_2O_3) is widely used as an ultra-wide bandgap semiconductor in emerging optoelectronics. Recent works show that Ga_2O_3 could be a promising high-κ dielectric material due to its high thermal stability, excellent moisture resistance, and ease of processing from solution phase. However, the dielectric properties of pristine Ga_2O_3 could be further improved. Here, aqueous-solution-synthesized Ga_2O_3 with excellent dielectric properties are achieved by phosphorus (P) incorporation. Using an Ga_2O_3 dielectric with optimal P (20 at. %) incorporation, oxide thin-film transistors (TFTs) exhibit enhanced performance with a mobility of $20.49 \pm 0.32\ cm^2\ V^{-1}\ s^{-1}$, subthreshold swing of 0.15 ± 0.01 V/dec, current on/off ratio $>10^6$, and superior bias stress stability. Systematic analyses show that proper P incorporation considerably reduces oxygen-related defects (oxygen vacancies and hydroxyls) in Ga_2O_3, resulting in better dielectric and TFT performance.

Gallium oxide (Ga_2O_3) is a rising star for next-generation high power electronics and solar-blind ultraviolet photodetectors because of its unique material properties and substrate availability.[1–4] While Ga_2O_3 is most investigated as an ultra-wide bandgap semiconductor, recent works by the authors and others found that Ga_2O_3 could be a promising high-κ dielectric for high-end transistors due to its large breakdown electric field of 8 MV/cm, a decent dielectric constant of ~10, good thermal/chemical stability, and especially high moisture resistance.[5–9]

It is worth noting that moisture absorption resistance is a major concern for high-κ oxides since a wet process is included in the current standard microelectronic fabrication.[10–15] Some high-κ oxides such as La-based oxide show relatively high permittivity and large bandgap; however, their high moisture absorption seriously damage the electrical performance and hinder practical applications.[10,11,13] Previous research indicates that moisture absorption might occur in the majority of high-κ oxides.[11] The Gibbs free energy change (ΔG) in the material was used to characterize the hygroscopicity of high-κ oxides.[11–13] High-κ oxides with positive ΔG could greatly suppress moisture absorption.[11–13] According to the previous theoretical calculations, among high-κ oxide materials, only Sc_2O_3 ($\Delta G = 38.2$ kJ mol^{-1}), Ga_2O_3 ($\Delta G = 23.1$ kJ mol^{-1}), and HfO_2 ($\Delta G = 20.5$ kJ mol^{-1}) have positive ΔG, indicating strong moisture resistance.[11–13] As a matter of fact, Ga_2O_3 has widely been used as a passivation material in microelectronics.[12] The high positive ΔG of Ga_2O_3 also indicates that solution processing is possible since exposure to moisture and air is inevitable. Our previous works, indeed, showed that a high-quality Ga_2O_3 dielectric thin-film could be made by a facile aqueous solution route, enabling potential low-cost and large-scale applications.[5,6]

However, the dielectric performance especially the leakage current and breakdown strength of solution-processed Ga_2O_3 need to be further improved. Doping is a simple and effective way to increase the

dielectric properties of Ga_2O_3. Unfortunately, related progress was quite slow. Oleksak *et al.* showed that W-doping could improve the dielectric characteristics (leakage current and breakdown strength) of Ga_2O_3, but thin-film transistors (TFTs) have not been demonstrated.[9] He *et al.* demonstrated that doping with Al could enhance the leakage current of pristine Ga_2O_3; however, the resulting TFTs showed relative poor on/off current ratio ($\sim 10^4$).[8] This group recently discovered that putting boron (B) into Ga_2O_3 improves dielectric quality and enables high-performance oxide TFTs.[7]

In this contribution, we report an expeditious aqueous approach to further enhance the Ga_2O_3 dielectric performance via phosphorus (P) incorporation. The role of P incorporation is characterized by a battery of physical techniques. The results reveal that proper P incorporation reduces oxygen-related defects [oxygen vacancies (V_O) and hydroxyls (–OH)], resulting in improved dielectric characteristics. Using an optimal Ga–P–O as gate dielectric, oxide TFTs exhibit enhanced performance, including a mobility (μ) of 20.49 ± 0.32 $cm^2\ V^{-1}\ s^{-1}$, subthreshold swing (*SS*) of 0.15 ± 0.01 V/dec, on/off ratio (I_{on}/I_{off}) of 1.9×10^6, threshold voltage (V_{TH}) of 0.03 ± 0.01 V, low-operation-voltage of 2 V, negligible hysteresis, and excellent bias-stress-stability.

The Ga–P–O solutions for spin-casting were prepared by mixing $Ga(NO)_3{\cdot}xH_2O$ and H_3PO_4 into DI water. The total concentration of metal precursors was 2 M and the atomic ratio of (P/Ga+P) was 0, 10, 20, 30, and 40 at. %, respectively. The In_2O_3 channel material was made by dissolving 0.1 M $In(NO)_3{\cdot}xH_2O$ in DI water. Prior to spin-casting, the formulated solution was rigorously stirred filtered through a 0.22-μm membrane filter. For the fabrication of oxide TFTs, a bottom gate top contact arrangement was used. The Ga–P–O solutions were spun on the P^{++}–Si wafers (used as a gate electrode) with a spin speed of 4500 rpm for 20 s. The Ga–P–O samples were subsequently annealed at 500 °C for 1 h. Then, the In_2O_3 solution was spun on the Ga–P–O/P^{++}–Si substrate at 3500 rpm, followed by 350 °C annealing for 1 h. Thermal evaporation was used to deposit 100 nm thick Al source and drain electrodes on In_2O_3 channel layers, resulting in a channel length/width of 100/1500 μm, respectively. In addition, an Al/Ga–P–O/P^{++}–Si metal–insulator–metal (MIM) structure was also fabricated to access the dielectric performance of Ga–P–O. The thermal behavior of Ga–P–O was observed by thermogravimetric analysis (TGA) and differential scanning calorimetry (DSC) (Netzsch). The Ga–P–O structures were investigated using grazing incidence X-ray diffraction (GIXRD) (Rigaku). The surface morphologies and chemical compositions were examined by AFM (Bruker) and XPS (Thermofisher). Ellipsometry (J. A. Woollam) was used to determine the refractive index and thickness of Ga–P–O films. The microstructures of the TFT device were observed by TEM (Tecnai). Electrical characterization was performed by a semiconductor parameter analyzer (Keithley 2614B) and an impedance analyzer (Keysight E4980A) in ambient condition.

Table I summarizes the results of a battery of characterization procedures used to assess the effect of P incorporation. Figure 1(a) shows the TGA and DSC curves of Ga–P–O precursor powder. The first endothermic peak at 135 °C was related to the dehydration of H_3PO_4.[7] The second peak position at 173 °C was attributed to dehydroxylation of gallium hydroxide.[5] TGA and DSC results suggest that the impurities could be completed decomposed at 500 °C and metal oxide framework could be formed. As a consequence, the annealing temperature is set at 500 °C.

Figure 1(b) shows the GIXRD patterns of the Ga–P–O films with P doping contents of 0–40 at. %. All the P doped Ga_2O_3 films exhibited an amorphous state. In general, an amorphous structure is preferred for a dielectric material due to the smooth surface, excellent channel/dielectric interface, and low leakage current in the absence of grain boundaries.[14] AFM images in Fig. 1(c) indicate extremely smooth surfaces of Ga–P–O films. The RMS roughness of 0, 10, 20, 30, and 40 at. % P doped Ga–P–O thin films were 0.190, 0.148, 0.172, 0.186, and 0.181 nm, respectively. Such atomically smooth morphology is essential for high-performance electronic device.[16]

The thickness and refractive index of the P-doped Ga_2O_3 films were estimated using ellipsometry. The 0, 10, 20, 30, and 40 at. % P-doped Ga_2O_3 thin films have thicknesses of 58.09, 57.85, 56.15, 54.56, and 53.50 nm, respectively. The film thickness declines slightly with the rise of P doping content, which could be due to the different $Ga(NO)_3{\cdot}xH_2O$ and H_3PO_4 precursors viscosities. Figure 1(d) shows the dispersion of the refractive index for the deposited Ga–P–O films. The pristine Ga_2O_3 film has a refractive index of 1.680 (at 550 nm), which is comparative to the previous reported value. The refractive index increases to 1.697 and 1.699 for 10 at. % and 20 at. % P-doping and then decreases to 1.688 and 1.675 for 30 at. % and 40 at. % P-doping. Note that refractive index is directly related to the film density.[17] The thin-film density for 0, 10, 20, 30, and 40 at. % P is calculated to be 4.87, 4.95, 4.96, 4.91, and 4.85 g/cm^3, respectively.[7,17] Therefore, suitable P-doping could increase the film density. This is due to the stronger P–O bonding (599.1 kJ/mol) than that of Ga–O (353.5 kJ/mol), which could improve the metal–oxygen–metal structure.[18] Moreover, the network-forming oxygen anions (PO_4^{3-}) can reduce oxygen-related defects (V_O and –OH) in the films, thereby increasing the film density. This will be discussed in the following paragraphs. However, too much P-doping would lower the film density since excess PO_4^{3-} will cause disruption of the original Ga_2O_3 networks.[19]

TABLE I. Summary of Ga–P–O thin-films properties with different P-doping ratios.

P-doping ratio (at. %)	Thickness (nm)	Roughness (nm)	Refractive index at 550 nm	Film density (g/cm^{-3})	(P/P + Ga) in film (%)	Areal capacitances at 100 Hz (nF/cm^2)	κ	Leakage current density at 3 MV/cm (A/cm^2)
0	58.09	0.190	1.680	4.87	0	154.8	10.16	68.98
10	57.85	0.148	1.697	4.95	7.4	151.6	9.90	1.38×10^{-5}
20	56.15	0.172	1.699	4.96	12.4	137.7	8.73	1.92×10^{-7}
30	54.56	0.186	1.688	4.91	18.5	128.9	7.94	5.23×10^{-7}
40	53.50	0.181	1.675	4.85	24.8	127.6	7.71	6.97×10^{-5}

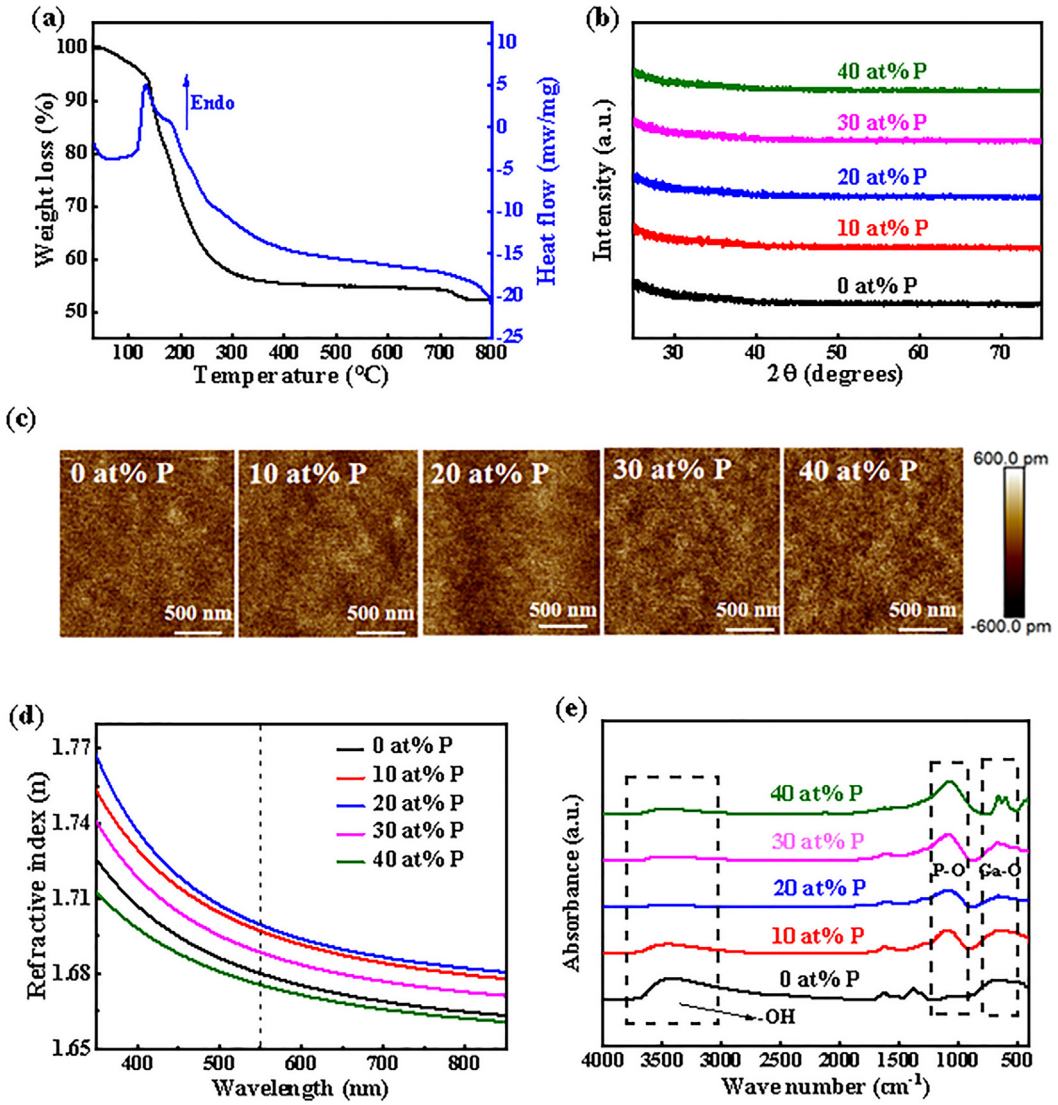

FIG. 1. (a) TGA and DSC curves, (b) GIXRD patterns, (c) AFM images, (d) dispersion of the refractive index, and (e) FTIR spectra of Ga–P–O with different P doping contents.

We have measured the refractive indexes of the prepared Ga_2O_3 thin films with different P incorporation contents in a long wavelength region (>350 nm). However, the distinctive dispersion of the P-doped Ga_2O_3 films has not been deeply studied. Bao *et al.* developed a newly model to study the sub-bandgap refractive indexes and optical properties of Si-doped β-Ga_2O_3 thin films.[20,21] They showed that the dispersion relationship of the refractive index in the sub-bandgap energy is as follows:[20,21]

$$n(E) = n_0 + \frac{E_1 - \sqrt{E_2(E_c - E)}}{E} \quad (1)$$

where E_1 and E_2 should be two energy parameters related to the material, while E_c should be the effective optical bandgap of the material, E is the photon energy ($E = hc/\lambda$), and n_0 is the static refractive index. The newly developed model is supposed to fit well with the experimental data and could explain the decrease in the refractive index with the increase in the wavelength. More detailed research on this model can be referred to Bao's work.[20,21]

To further clarify that P incorporation can give high-quality films, FTIR measurements were performed, as shown in Fig. 1(e). The peak in the range of 684–463 cm^{-1} is related to the stretching vibration of the Ga–O bond.[6] The peak in the range of 900–1200 cm^{-1} is related to the stretching vibration of the P–O bond.[22] The broad peak in the range 3000–3700 cm^{-1} corresponds to hydroxyl (–OH) group stretching vibrations.[23] After P incorporation, P–O bond is formed and the content of hydroxyls (–OH) in the pristine Ga_2O_3 film decrease with 20 at. % P shows the best results.

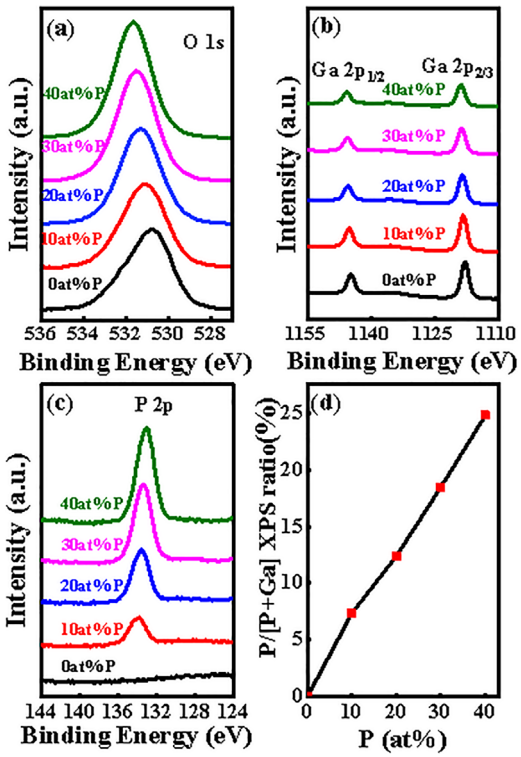

FIG. 2. XPS spectra for the Ga–P–O films with different P doping contents. (a) O 1s, (b) percentage of corresponding O components, (c) Ga 2p, (d) P 2p spectra, and (e) P doping ratio between solution and film.

The chemical and defect states of the Ga–P–O were monitored using XPS. As shown in Figure 2(a), the O 1s binding energy increases as the P-doping ratio increases, from 530.7 eV for pristine Ga_2O_3 to 531.6 eV for 40% P-doped Ga_2O_3. Previous reports have shown that the characteristic binding energy for oxyanions (PO_4^{3-}) is ~520 eV.[24–26] Therefore, the positive shifts of O 1s peak upon P-doping suggest the existence of oxyanions (PO_4^{3-}) in the final Ga_2O_3 thin film. Figure 2(b) depicts the Ga 2p spectra. The production of Ga_2O_3 was confirmed by the observation of two spin–orbital bimodal Ga $2p_{1/2}$ and Ga $2p_{3/2}$ with a space of 27 eV.[6] The geometries and binding energies of Ga peaks remain intact, indicating that the local environment and oxidation state of Ga^{3+} are unaffected by the addition of P.[6] The corresponding P 2p spectra were demonstrated in Fig. 2(c). Previous reports have summarized the P 2p peak energies.[27] The peaks at ~135.6, 133.5, 128.6, and 129.9 eV correspond to P_2O_5, phosphate, phosphide, and elemental P, respectively.[27] Therefore, in the present work, the characteristic peak at ~133.5 eV is assigned to phosphate (PO_4^{3-}, positively charged P^{5+} ion with four oxygen atoms around it). The characteristic peak at ~128.6 eV for P^{3-} (phosphide, metal–phosphorus bond) is absent. This further verifies the existence of oxyanions (PO_4^{3-}) in the resulting Ga_2O_3 film. In addition, as shown in Fig. 2(d), the P/Ga + P ratio in the thin-film steadily increases from 0 to 7.4, 12.4, 18.5, and 24.8%, as the P ratio in the precursor increases from 0 to 10%, 20%, 30%, and 40%, respectively.

Figure 3 illustrates the formation mechanism for Ga_2O_3 upon P incorporation (in the form of phosphoric acid). As shown in Fig. 3(a), for gallium nitrate in the aqueous solution, Ga cation usually exists [$Ga(OH_2)_6^{3+}$].[5] These aquo-ligands undergo thermohydrolysis in the post-annealing fabrication and form the metal–oxygen–metal (M–O–M) framework.[28] However, oxygen-related defects (V_O and –OH) are inevitably existed in the final Ga_2O_3 due to incomplete condensation.[14] These defects are the major sources for the poor dielectric performance in typical sol-gel high-κ oxides.[12] As shown in Fig. 3(b), the incorporation of phosphoric acid usually forms phosphate (PO_4^{3-}) in the solution.[28,29] By replacing part of the aquo-ligands, these oxyanions have a strong complexing capacity with adjacent Ga cations.[28,29] This behavior could effectively reduce the –OH groups.[28,29] On the other hand, the oxyanions (PO_4^{3-}) also provide additional oxygen atoms and, therefore, could reduce V_O.[28,29] In addition, the PO_4^{3-} themselves also act as network formers by forming M–O–P–O–M bonds in the Ga_2O_3 lattice.[28] Since the P–O bonding (599.1 kJ/mol) is higher than Ga–O (353.5 kJ/mol), the network-forming oxyanions are believed to be stable.[18]

To investigate the dielectric characteristics of P doped Ga_2O_3 layers, MIM structure capacitors based on Al/Ga–P–O/P^{++}–Si were created. Figure 4(a) depicts the capacitance–frequency (C–f) characteristics at 10^2–10^5 Hz. The dielectric constants of the 0, 10, 20, 30, and 40 at. %-P doped Ga_2O_3 are calculated to be 10.16, 9.90, 8.73, 7.94, and 7.71, respectively. The decrease in the dielectric constant could be

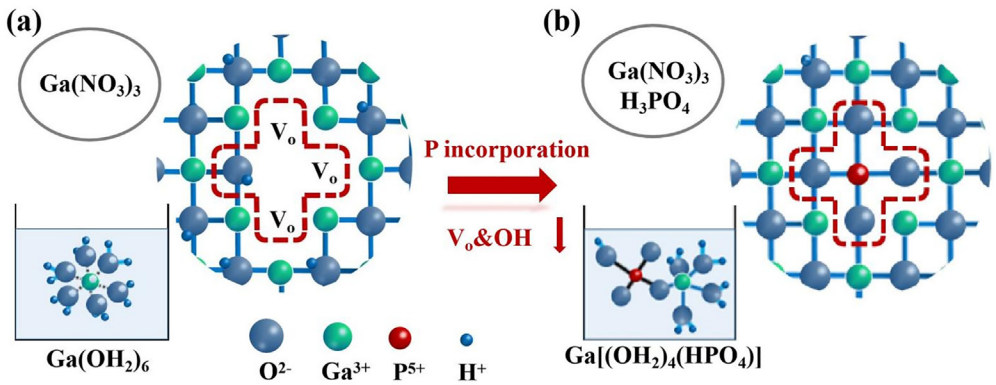

FIG. 3. Schematic diagram of (a) aqueous-solution-synthesized Ga_2O_3 and (b) after phosphoric acid incorporation.

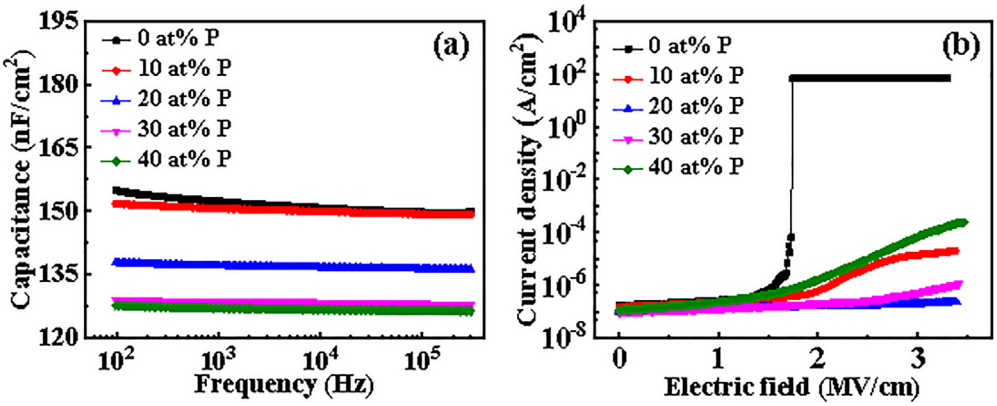

FIG. 4. (a) Capacitance–frequency and (b) current–voltage characteristics of the Ga–P–O films with P doping contents of 0–40 at. %.

attributed to the reduction of "–OH" impurity.[30] Note that the P-doing samples show weaker frequency dispersion, which is due to the enhanced film quality as will be discussed further below.[30] Figure 4(b) showed the leakage current density vs electric field (J–E) of the Ga–P–O insulator. Upon P doping, the leakage current density and the breakdown electric field are tremendously improved. As the P doping ratio increases to 20%, the Ga–P–O dielectric shows the lowest leakage current of 1.92×10^{-7} A/cm^2 at 3 MV/cm. Note that all the Ga–P–O films showed similar excellent morphologies, the enhanced leakage current performance should be related to the microstructural details. Generally, the oxygen-related defects in high-κ oxides would result in deep-trap levels for electron activation and deteriorate dielectric properties.[31] The above-mentioned film characterization suggests that the improvement is attributed to the reduction in oxygen-related defects (V_O and –OH) upon P-doping. Moreover, P-doping also increases the thin-film density and reduces the voids in the neat Ga_2O_3 which is also the cause of the relatively high leakage current. However, further increase in the P-doping ratio to 40 at. % would do harm to the electrical performance, which is directly related to excess phosphate (PO_4^{3-}) due to the formation of non-bridging oxygen atoms, causing disruption of the original Ga_2O_3 networks.[19]

The structural diagram and cross-sectional TEM of In_2O_3/Ga–P–O (20 at. % P) device were demonstrated in Figs. 5(a) and 5(b). The TEM image reveals well defined and excellent uniform In_2O_3/Ga–P–O and Ga–P–O/Si interfaces, which is essential for carrier transport of the TFT device. The thicknesses of Ga–P–O and In_2O_3 are 60 and 6 nm measured by TEM, in accordance with the ellipsometry analysis. Next, all aqueous-solution-processed In_2O_3 TFTs with Ga–P–O insulating layers were fabricated to investigate the impacts of P-doping. Figures 5(c) and 5(d) show the representative transfer and output curves for In_2O_3/Ga–P–O TFTs with different P-doping contents, with average device operating parameters summarized in Table II.

For the calculation of mobility, we can extract it according to the following formula:[32]

$$\mu_{\text{sat}} = \frac{2L}{C_{ox}W}\frac{I_{Dsat}}{(V_G - V_T)^2}, \tag{2}$$

where C_{ox} is the capacitance per unit area of the dielectric layer, V_T is the threshold voltage, V_G is the gate voltage, and W and L are the channel width and length, respectively.

For the interface trap density, we can first obtain the threshold swing (SS) according to Eq. (3) and then calculate the interface defect density (D_{it}) through SS according to Eq. (4)[33]

$$SS = \left(\frac{d\log_{10}I_{DS}}{dV_{GS}}\bigg|_{\max}\right)^{-1}, \tag{3}$$

$$D_{it} = \left(\frac{q \cdot SS \cdot \log(e)}{k_B T} - 1\right)\frac{C_{ox}}{q}, \tag{4}$$

where q is the amount of the electron charge, e is the natural constant, k_B is the Boltzmann constant, T is the thermodynamic temperature of the device, and C_{ox} is the unit capacitance of the insulating layer.

The In_2O_3 TFTs comprising the neat Ga_2O_3 dielectrics showed a modest μ of 12.13 ± 0.18 cm^2 V^{-1} s^{-1} and I_{on}/I_{off} of 7.6×10^5. These operating parameters are in line with our recent reports based on a similar processing. However, the TFT device mobility gradually increases with the rise of P-doping ratio in Ga_2O_3 dielectrics and reaches a maximum μ value of 20.49 ± 0.32 cm^2 V^{-1} s^{-1} and I_{on}/I_{off} of 1.9×10^6 for 20 at. % P-doping ratio. The enhancement of μ also leads to the increase in I_{on} and hence I_{on}/I_{off} ratio, which is also reflected in the output characteristics [Fig. 4(d)]. Previous reports showed that inherent oxygen-related defects (mainly –OH and V_O) in high-κ oxides usually act as electron trapping sites, deteriorating carrier transport.[6,7,16,31] This is the reason why pristine Ga_2O_3-gated device showed a relatively low mobility. Suitable P-doping could effectively reduce the oxygen-related defects in neat Ga_2O_3, leading to the enhancement of device mobility. However, the device mobility falls to 14.22 ± 0.25 cm^2 V^{-1} s^{-1} as the P-doping content further increases to 40 at. % since excess phosphate (PO_4^{3-}) may act as impurities and cause disruption of the original Ga_2O_3 networks.[19] The device mobility trend is in accordance with the above-mentioned microstructural, capacitance–frequency, and leakage current analyses. In_2O_3 TFTs with optimal P content of 20 at. % exhibited μ of 20.49 ± 0.32 cm^2 V^{-1} s^{-1}, I_{on}/I_{off} of 1.9×10^6, SS of 0.15 ± 0.01 V/dec, V_{TH} of 0.03 ± 0.01 V, and negligible hysteresis. Moreover, the device could be operated in a low-operation-voltage (~2 V), which is important for low-power portable mobile electronic systems. It is worth nothing that the In_2O_3/Ga–P–O TFTs performance is among the state-of-the-art devices based on fully solution-processing.[12–15]

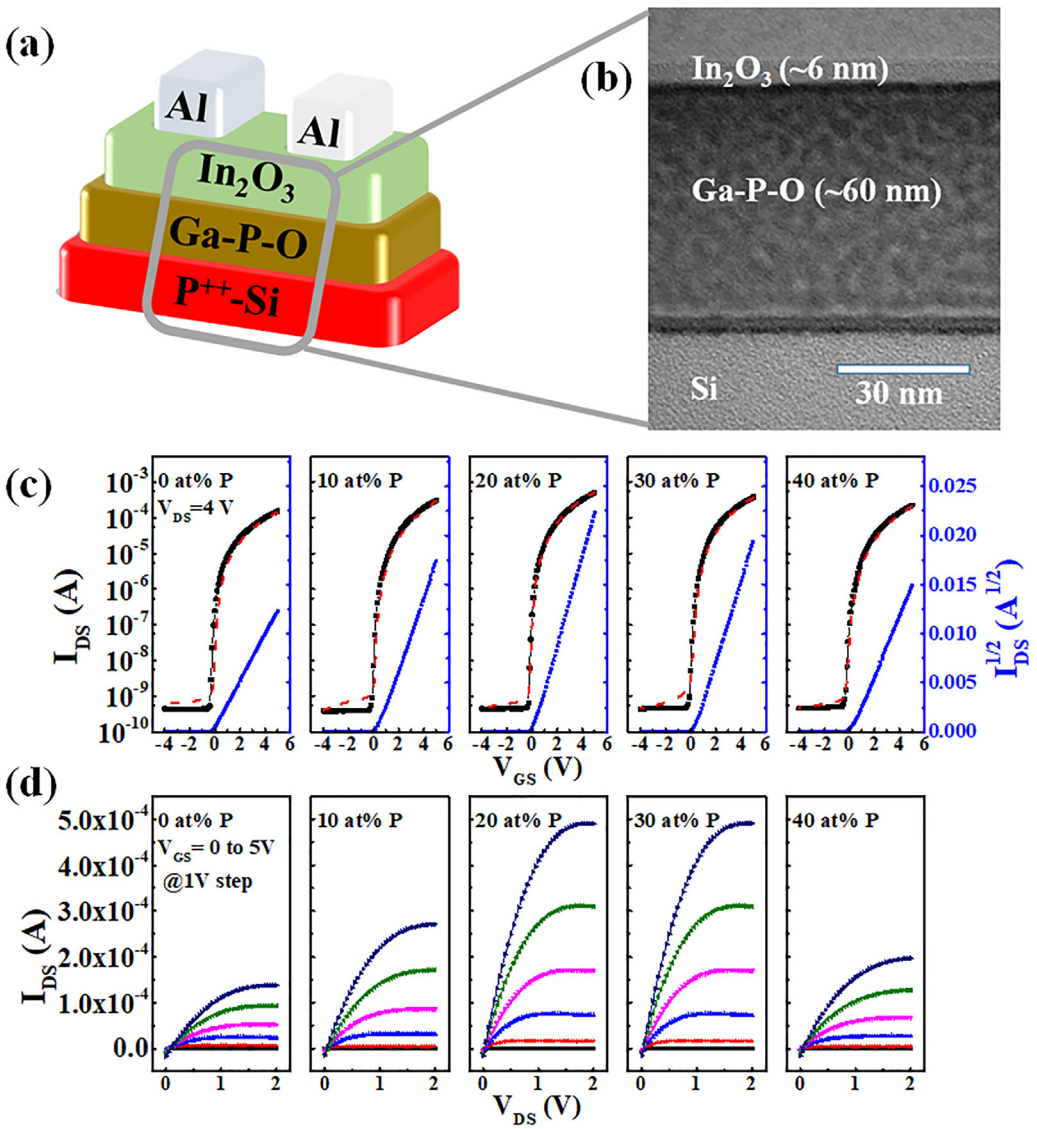

FIG. 5. (a) Structural diagram and (b) cross-sectional TEM of In_2O_3/Ga–P–O (20 at. % P) TFT device. (c) Transfer and (d) output curves for aqueous-based In_2O_3/Ga–P–O TFTs with P doping contents of 0–40 at. %.

TABLE II. Summary of device parameters for In_2O_3 TFTs with indicated Ga–P–O dielectrics. Average values of 15 devices.

P-doping ratio (at. %)	Mobility ($cm^2\ V^{-1}\ s^{-1}$)	On/off current ratio	Threshold voltage (V)	Subthreshold swing (V/dec)	Interface trap densities ($cm^{-2}{\cdot}eV^{-1}$)
0	12.13 ± 0.18	7.6×10^5	-0.12 ± 0.01	0.10 ± 0.01	1.52×10^{12}
10	15.90 ± 0.24	1.2×10^6	0.11 ± 0.02	0.15 ± 0.01	1.28×10^{12}
20	20.49 ± 0.32	1.9×10^6	0.03 ± 0.01	0.15 ± 0.01	1.33×10^{12}
30	17.75 ± 0.29	8.7×10^5	0.25 ± 0.04	0.14 ± 0.01	1.23×10^{12}
40	14.22 ± 0.25	6.4×10^5	0.19 ± 0.03	0.16 ± 0.02	1.30×10^{12}

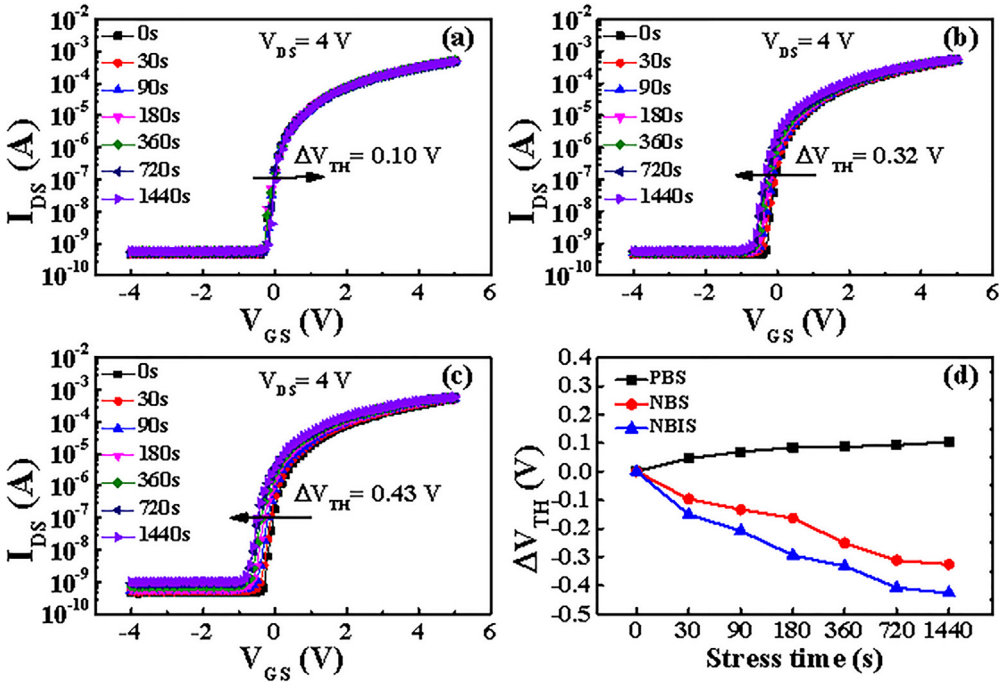

FIG. 6. In_2O_3/Ga–P–O (20 at. % P) TFTs transfer curves under (a) PBS ($V_G = 2$ V), (b) NBS ($V_G = -2$ V), (c) NBIS ($V_G = -2$ V), and (d) the corresponding threshold voltage shifts.

The bias stress stability of In_2O_3 TFTs based on optimized Ga–P–O (20 at. % P) dielectrics was evaluated and shown in Fig. 6. Figure 6(a) shows the positive bias stress (PBS) instability of the device. A small positive V_{TH} shift (0.1 V after gate-bias-stress of 2 V for 1440 s) was observed, which is attributed to charge trapping behavior occurring in gate dielectrics and/or at the dielectrics/channel interface. In addition, for bottom-gate devices without passivation, the adsorption of oxygen molecules also contributed to positive V_{TH} shift. Figure 6(b) demonstrated the negative bias stress (NBS) instability of the In_2O_3/Ga–P–O TFTs. A small negative V_{TH} shift (−0.32 V after gate-bias-stress of −2 V for 1440 s) was observed, due to hole trapping at the dielectric or dielectrics/channel interface as well as moisture adsorbed reaction at the back channel.[7] Figure 6(c) illustrates the negative bias illumination stress (NBIS) instability of the oxyanion-incorporated device. It is shown that under illumination, photoexcited holes would drift to the dielectric or dielectric/semiconductor interface, leading to much more serious V_{TH} shift of −0.43 V.[7] The corresponding V_{TH} shifts of the P-doped devices under PBS, NBS, and NBIS were drawn in Fig. 5(d). It is noteworthy that the P-doped Ga_2O_3-gated TFTs show prominent improvements under bias stress compared with the previous reports on pristine Ga_2O_3 or B-doped Ga_2O_3-gated device, due to the reduced contents of oxygen-related defects in the films.[5–7] Moreover, the diffusion of P from initial Ga_2O_3 into the In_2O_3 layer may help to passivate the oxygen vacancy/hydroxyl-related defects in In_2O_3 due to the formation of a more stable In–O–P–O–In metal network (similar to the role of P doping in Ga_2O_3), thereby improving the overall electrical performance and stability of device. We believe that the principle illustrated here by the incorporation of phosphoric acid is applicable to other high-κ oxides for a wide variety of applications.

In summary, a simple method for improving the dielectric and TFT performance of aqueous-solution-derived Ga_2O_3 with phosphoric acid addition is reported. It is found that appropriate P incorporation acts as network connections (in the form of PO_4^{3-}) and reduces the oxygen-related defects (V_O and –OH) in undoped Ga_2O_3. Metal oxide TFTs exhibit excellent electrical characteristics including μ of 20.49 ± 0.32 $cm^2 V^{-1} s^{-1}$, SS of 0.15 ± 0.01 V/dec, $I_{on}/I_{off} > 10^6$, negligible hysteresis, and enhanced stability when employing Ga_2O_3 dielectric with proper P (20 at. %) incorporation. This work presents a route for next-generation of low-cost advanced Ga_2O_3-based device.

This work was supported by the National Natural Science Foundation of China (Nos. 61704111 and 62001308) and the Pearl River Talents Plan of Guangdong Province (No. 2017GC010092). Yu Zhang thanks the support from Lihu Elite project (No. LHRC20220403b).

AUTHOR DECLARATIONS

Conflict of Interest

The authors have no conflicts to disclose.

Author Contributions

Wangying Xu: Conceptualization (equal); Formal analysis (equal); Funding acquisition (equal); Investigation (equal); Methodology (equal); Project administration (equal); Supervision (equal); Writing – original draft (equal); Writing – review & editing (equal). **Deliang Zhu:** Writing – review & editing (equal). **Tao Peng:** Investigation (equal). **Lin Chen:** Investigation (equal). **Weicheng Huang:** Formal

analysis (equal). **Shuangmu Zhuo:** Writing – review & editing (equal). **Qiubao Lin:** Writing – review & editing (equal). **Chun Zhao:** Supervision (equal); Writing – review & editing (equal). **Fang Xu:** Writing – review & editing (equal). **Yu Zhang:** Writing – review & editing (equal).

DATA AVAILABILITY

The data that support the findings of this study are available from the corresponding authors upon reasonable request.

REFERENCES

[1]J. Zhang, J. Shi, D.-C. Qi, L. Chen, and K. H. Zhang, APL Mater. **8**(2), 020906 (2020).
[2]C. L. Wang, J. C. Zhang, S. R. Xu, C. F. Zhang, Q. Feng, Y. C. Zhang, J. Ning, S. L. Zhao, H. Zhou, and Y. Hao, J. Phys. D **54**(24), 243001 (2021).
[3]C. Xie, X.-T. Lu, X.-W. Tong, Z.-X. Zhang, F.-X. Liang, L. Liang, L.-B. Luo, and Y.-C. Wu, Adv. Funct. Mater. **29**(9), 1806006 (2019).
[4]X. H. Chen, F. F. Ren, S. L. Gu, and J. D. Ye, Photonics Res. **7**(4), 381–415 (2019).
[5]W. Xu, H. Cao, L. Liang, and J. B. Xu, ACS Appl. Mater. Interfaces **7**(27), 14720–14725 (2015).
[6]L. Chen, W. Xu, W. Liu, S. Han, P. Cao, M. Fang, D. Zhu, and Y. Lu, ACS Appl. Mater. Interfaces **11**(32), 29078–29085 (2019).
[7]W. Xu, L. Chen, S. Han, P. Cao, M. Fang, W. Liu, D. Zhu, and Y. Lu, J. Phys. Chem. C **124**(14), 8015–8023 (2020).
[8]F. He, Y. Wang, Z. Lin, J. Su, J. Zhang, J. Chang, and Y. Hao, Appl. Phys. Lett. **119**(11), 112102 (2021).
[9]R. P. Oleksak, W. F. Stickle, and G. S. Herman, J. Mater. Chem. C **3**(13), 3114–3120 (2015).
[10]Y. Zhao, M. Toyama, K. Kita, K. Kyuno, and A. Toriumi, Appl. Phys. Lett. **88**(7), 072904 (2006).
[11]Y. Zhao, K. Kita, and A. Toriumi, Appl. Phys. Lett. **96**(24), 242901 (2010).
[12]B. Wang, W. Huang, L. Chi, M. Al-Hashimi, T. J. Marks, and A. Facchetti, Chem. Rev. **118**(11), 5690–5754 (2018).
[13]A. Liu, H. Zhu, H. Sun, Y. Xu, and Y. Y. Noh, Adv. Mater. **30**, e1706364 (2018).
[14]W. Xu, H. Li, J. B. Xu, and L. Wang, ACS Appl. Mater. Interfaces **10**(31), 25878–25901 (2018).
[15]S. Park, C.-H. Kim, W.-J. Lee, S. Sung, and M.-H. Yoon, Mater. Sci. Eng., R **114**, 1–22 (2017).
[16]X. Zhuang, S. Patel, C. Zhang, B. Wang, Y. Chen, H. Liu, V. P. Dravid, J. Yu, Y. Y. Hu, W. Huang, A. Facchetti, and T. J. Marks, J. Am. Chem. Soc. **142**(28), 12440–12452 (2020).
[17]J. H. Park, Y. B. Yoo, K. H. Lee, W. S. Jang, J. Y. Oh, S. S. Chae, H. W. Lee, S. W. Han, and H. K. Baik, ACS Appl. Mater. Interfaces **5**(16), 8067–8075 (2013).
[18]S. Parthiban and J.-Y. Kwon, J. Mater. Res. **29**(15), 1585–1596 (2014).
[19]F. Tourtin, P. Armand, A. Ibanez, and E. Philippot, J. Solid State Chem. **134**(1), 91–98 (1997).
[20]Y. Bao, X. Wang, and S. Xu, J. Semicond. **43**(6), 062802 (2022).
[21]Y. Bao and S. Xu, J. Phys. D **54**(15), 155102 (2021).
[22]B. Yuan, W. Xing, Y. Hu, X. Mu, J. Wang, Q. Tai, G. Li, L. Liu, K. M. Liew, and Y. Hu, Carbon **101**, 152–158 (2016).
[23]K. N. Woods, T. H. Chiang, P. N. Plassmeyer, M. G. Kast, A. C. Lygo, A. K. Grealish, S. W. Boettcher, and C. J. Page, ACS Appl. Mater. Interfaces **9**(12), 10897–10903 (2017).
[24]J. Chastain and R. C. King, Jr., *Handbook of X-ray Photoelectron Spectroscopy* (Perkin-Elmer Corporation, 1992), Vol. 40, p. 221.
[25]C. Viornery, Y. Chevolot, D. Léonard, B.-O. Aronsson, P. Péchy, H. J. Mathieu, P. Descouts, and M. Grätzel, Langmuir **18**(7), 2582–2589 (2002).
[26]R. K. Brow, J. Non-Cryst. Solids **194**(3), 267–273 (1996).
[27]J. F. Wager, D. L. Ellsworth, S. M. Goodnick, and C. W. Wilmsen, J. Vac. Sci. Technol. **19**(3), 513–518 (1981).
[28]H. Park, Y. Nam, J. Jin, and B.-S. Bae, J. Mater. Chem. C **2**(30), 5998 (2014).
[29]W. W. Rudolph, D. Fischer, M. R. Tomney, and C. C. Pye, Phys. Chem. Chem. Phys. **6**(22), 5145–5155 (2004).
[30]W. Xu, H. Wang, F. Xie, J. Chen, H. Cao, and J.-B. Xu, ACS Appl. Mater. Interfaces **7**(10), 5803–5810 (2015).
[31]X. Zhang, B. Wang, W. Huang, Y. Chen, G. Wang, L. Zeng, W. Zhu, M. J. Bedzyk, W. Zhang, and J. E. Medvedeva, J. Am. Chem. Soc. **140**(39), 12501–12510 (2018).
[32]E. Fortunato, P. Barquinha, and R. Martins, Adv. Mater. **24**(22), 2945–2986 (2012).
[33]D. Luo, L. Lan, M. Xu, H. Xu, M. Li, L. Wang, and J. Peng, J. Electrochem. Soc. **159**(5), H502–H506 (2012).